

Spatial Adaptation Layer: Interpretable Domain Adaptation For Biosignal Sensor Array Applications

Joao Pereira, Michael Alummoottil, Dimitrios Halatsis and Dario Farina, *Fellow, IEEE*
Neuromechanics and Rehabilitation Technology Group, Imperial College London, London W12 0BZ, UK

Abstract—Biosignal acquisition is key for healthcare applications and wearable devices, with machine learning offering promising methods for processing signals like surface electromyography (sEMG) and electroencephalography (EEG). Despite high within-session performance, intersession performance is hindered by electrode shift, a known issue across modalities. Existing solutions often require large and expensive datasets and/or lack robustness and interpretability. Thus, we propose the Spatial Adaptation Layer (SAL), which can be prepended to any biosignal array model and learns a parametrized affine transformation at the input between two recording sessions. We also introduce learnable baseline normalization (LBN) to reduce baseline fluctuations. Tested on two HD-sEMG gesture recognition datasets, SAL and LBN outperform standard fine-tuning on regular arrays, achieving competitive performance even with a logistic regressor, with orders of magnitude less, physically interpretable parameters. Our ablation study shows that forearm circumferential translations account for the majority of performance improvements, in line with sEMG physiological expectations.

Index Terms—biosignals, domain adaptation, interpretability, electrode shift

I. INTRODUCTION

BIOSIGNAL acquisition has powered a plethora of healthcare applications and wearable devices. Due to their complex structure, machine learning emerged as a promising method of leveraging biosignal information, such as movement intent classification from surface electromyography (sEMG) and electroencephalography (EEG) for human machine interactions (HCI) [1].

Furthermore, sensor arrays enable the acquisition of spatially distributed information. Not only can this information be used for the inverse modelling of anatomically interpretable quantities, such as electrocardiography imaging (ECGi) [2] or EMG decomposition [3], but its regular structure also enables image-based processing [4] and deep learning approaches [5] to be applied for these downstream tasks.

While aforementioned methods often yield high performance within the same recording session, performance is generally impractically low across sessions [6]. The displacement of sensors across sessions, referred to as electrode shift, is a known contributor in sEMG [6], EEG [7], and function near-infrared spectroscopy (fNIRS) [8]. Some studies have aimed to learn representations invariant to electrode shift [9]. While

Meta Reality Labs has obtained remarkably low error across sessions and even subjects [1], it is dependent on a large dataset that can only be obtained through a resource intensive data collection effort, lacks interpretability, and only works on their own hardware, restricting it from external applications.

Beyond invariance learning, another solution proposed is calibrating to data from the new session. Image and signal processing methods have been used such as detecting anatomical landmarks for virtually reversing electrode displacement [4]. Other studies have attempted supervised domain adaptation techniques, such as the use of fine-tuning, progressive neural networks [10], and even model-agnostic meta-learning [11]. One promising approach introduces a 2-step domain adaptation procedure: where an RNN is used for training on one session, then a linear layer is used to map inputs to the input space of the previous session with frozen RNNs weights [12]. However, either signal processing approaches are highly dependent on heuristic choices and independent preprocessing steps, or learning based approaches are non-interpretable and require large amounts of adaptation data, limiting their applicability in settings that require very short adaptation sessions.

Therefore, in this paper we introduce the Spatial Adaptation Layer (SAL), inspired by Spatial Transformer Networks (STNs) [13]. While STNs compute coefficients of an affine transformation as a function of the input (localization network), SAL learns these parameters, decomposed into separable transformations for interpretability, via an adaptation session. Without a localization net, often a black box model, we bring further interpretability to the model. On top of SAL, we also subtract biases from each biosignal channel that are learned during adaptation to account for baseline activity fluctuations. Inspired by the baseline normalization (BN) procedure from [4], this method is referred as learnable BN (LBN).

The philosophy behind SAL is that transforming biosignal images from a new recording session back into the original spatial frame in which the original classifier was trained on would have a significant impact on the loss function. Consequently, parameters can be learned directly from the supervision loss during adaptation. Additionally, while STNs are most useful for handling i.i.d. affine transformations, SAL is especially designed for intersession adaptation, where learned patterns are connected across sessions via a single, unique affine transformation. While similar in structure to the 2-step adaptation introduced in [12], SAL uses far fewer parameters,

This project was supported by UK Research and Innovation [UKRI Centre for Doctoral Training in AI for Healthcare grant number EP/S023283/1], the Imperial-META Wearable Neural Interfaces Research Centre and the Onassis Foundation.

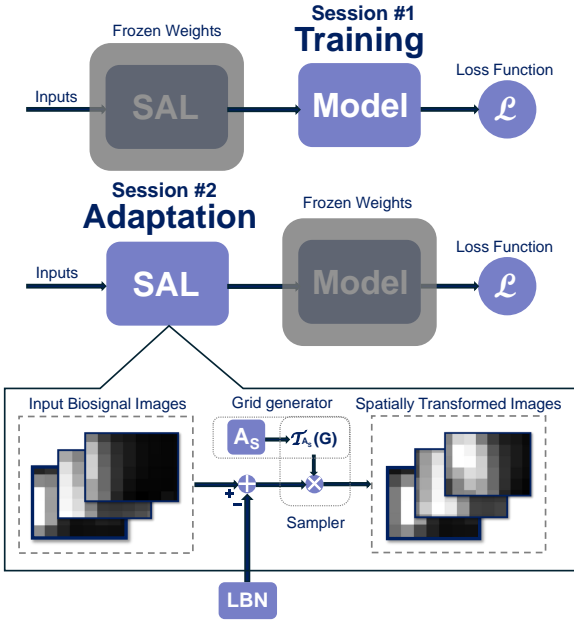


Fig. 1. Schematic of SAL architecture and usage. SAL weights are frozen and the chosen model is optimized on session #1. On session #2, given a few examples, the model is frozen and the parameters of SAL are optimized for adaptation. SAL is similar to an STN module from [13], with the key difference that rather than modelling affine coefficients A_s as a function of the input, A_s are treated as learnable parameters.

being directly interpretable as well as more efficient and regularizing. We evaluate our methods on two publicly available HD-sEMG datasets. For regular biosignal array images, our interpretable method offers higher performance than standard fine-tuning and is consistent with observations based on past sEMG studies.

II. METHODS & DATASETS

A. Spatial Adaptation Layer

In the Spatial Adaptation Layer, seen in Fig 1, we used the differentiable image sampling operator proposed in STNs [13] which they frame as resampling an image based on a set of sampling coordinates $T_{A_S}(G)$, given original grid coordinates of the image, G , under some affine transformation A_S . This can be seen in Eq. 1 with (x_i^s, y_i^s) elements of the sampling coordinates, and (x_i^t, y_i^t) elements of the target coordinates in G of the output image, $\forall i \in [1 \dots HW]$ for an image of dimensions $H \times W$:

$$\begin{pmatrix} x_i^s \\ y_i^s \end{pmatrix} = T_{A_S}(G_i) = A_S \begin{pmatrix} x_i^t \\ y_i^t \\ 1 \end{pmatrix} = \begin{pmatrix} \theta_{11} & \theta_{12} & \theta_{13} \\ \theta_{21} & \theta_{22} & \theta_{23} \end{pmatrix} \begin{pmatrix} x_i^t \\ y_i^t \\ 1 \end{pmatrix} \quad (1)$$

Given an input image U , the resampling to an output image V for a single channel is defined in Eq. 2 for some sampling kernel k with parameters Φ_x and Φ_y :

$$V_i = \sum_{n=1}^H \sum_{m=1}^W U_{nm} k(x_i^s - m; \Phi_x) k(y_i^s - n; \Phi_y) \quad (2)$$

For bilinear interpolation this can be written as:

$$V_i = \sum_{n=1}^H \sum_{m=1}^W U_{nm} \max(0, 1 - |x_i^s - m|) \max(0, 1 - |y_i^s - n|) \quad (3)$$

The authors in [13] show that the partial derivatives of the output image with respect to the input and sampling grid can be defined as:

$$\frac{\partial V_i}{\partial U_{nm}} = \sum_{n=1}^H \sum_{m=1}^W \max(0, 1 - |x_i^s - m|) \max(0, 1 - |y_i^s - n|) \quad (4)$$

$$\frac{\partial V_i}{\partial x_i^s} = \sum_{n=1}^H \sum_{m=1}^W U_{nm} \max(0, 1 - |y_i^s - n|) \begin{cases} 0, & |m - x_i^s| \geq 1 \\ 1, & m \geq x_i^s \\ -1, & m < x_i^s \end{cases} \quad (5)$$

yielding a sub-differentiable sampling mechanism, seen in Eq. 5. Gradients can flow through since $\frac{\partial x_i^s}{\partial \theta}$ and $\frac{\partial y_i^s}{\partial \theta}$ can be easily derived from Eq. 1, effectively allowing backpropagation to be applied. For more interpretable parameters to be learned, we further decompose A_S into sub-transforms whilst preserving differentiability in the operator. We do this by making use of transformations in homogenous coordinates such that the general affine transformation A is defined as Eq. 6 with T , R , S_c and S_h representing translation, rotation, scaling and shearing respectively.

$$\begin{aligned} A &= S_h S_c R T \\ &= \begin{pmatrix} 1 & sh_x & 0 \\ sh_y & 1 & 0 \\ 0 & 0 & 1 \end{pmatrix} \begin{pmatrix} s_x & 0 & 0 \\ 0 & s_y & 0 \\ 0 & 0 & 1 \end{pmatrix} \\ &\quad \begin{pmatrix} \cos \phi & -\sin \phi & 0 \\ \sin \phi & \cos \phi & 0 \\ 0 & 0 & 1 \end{pmatrix} \begin{pmatrix} 1 & 0 & T_x \\ 0 & 1 & T_y \\ 0 & 0 & 1 \end{pmatrix} \quad (6) \end{aligned}$$

Hence, we can redefine A_S as the submatrix of A such that $A_S = A[I, J]$ where $I = \{1, 2\}$ and $J = \{1, 2, 3\}$. Given tensor *slicing* and *multiplication* are differentiable operations, gradients are preserved with no loss of information and can be defined with respect to the sampling grid coordinates by applying the chain rule (e.g. $\frac{\partial x_i^s}{\partial T_x} = \frac{\partial x_i^s}{\partial \theta} \frac{\partial \theta}{\partial T_x}$). This affine transformation and layer is parametrised by 7 learnable parameters. Ordinarily, one would expect such parameters to be learned through a similarity metric applied to images directly as in image registration. However exact correspondence is ambiguous in our scenario. Instead, parameters can be learned for any optimization based downstream task. Here, classification loss is backpropagated for multiple windows during adaptation, guiding the learning of these physically meaningful parameters to uncover a unique mapping from session to session.

B. Datasets

Capgmyo [5]: Signals were acquired via eight differential, silver, wet electrode array evenly spaced around the circumference of the arm, resulting in 128 simultaneous channel recordings (irregular grid of 8x16) acquired at 1000 Hz. All experiments were carried out with data subset DBb, containing two recording sessions from subjects. Due to data corruption in the last subject's recordings, this experiment was carried forward with the first 9 subjects. Each session consisted of 10 repetitions of 8 isotonic and isometric hand and finger gestures ($G = 8$) held for 3-10s. As in [5], only the central 1s interval of each gesture was considered in this study.

CSL Dataset [4]: Bipolar recordings were acquired at 2048Hz via an electrode array with 192 electrodes with an inter-electrode distance of 10 mm and taking differences between consecutive samples, resulting in a regular grid of 7x24 (168 channels). This dataset contains recordings from 5 different subjects across 5 different days. For each recording, subjects performed 10 repetitions of 27 different gestures. To ensure that the labelled data corresponds to the desired movement, the activity segmentation from [4] was used to determine the active movement segment. The rest (idle) gesture was excluded.

C. Preprocessing & Classification

As in [5], signals were processed with a digital bandpass filter (20-380 Hz, fourth-order Butterworth) and power-line interference was reduced using a digital band-stop filter (45-55H Hz, fourth-order Butterworth). Activity images are used as in [4], where the root mean square (RMS) was obtained for each given channel. To obtain an instantaneous estimate of RMS, the raw sEMG activity is squared, then convolved with a moving average (MA) filter of length $2 * T_{RMS} + 1$, introducing a delay of T_{RMS} to the system, fixed to be 75ms. As in [5], we report majority voting accuracies for the full activity segment for CSL and 150ms windows for Capgmyo.

LBN is implemented as $b \in \mathbb{R}^{HW}$, representing negative biases applied at each input channel. Since a logistic regressor has its own biases per channel, and deep CNNs are known for their expressivity, LBN was not considered when using standard fine-tuning with all model parameters. To evaluate the effect of LBN, we implemented the baseline normalization (BN) procedure from [4], where the average RMS from each channel during the rest (idle) gesture was estimated and subtracted from the remaining gestures for a given session. This step aimed to enforce more consistent noise distributions across sessions. To prevent overfitting to noisy/corrupted channels during training, the effect of dropout at the input ($p = 0.5$) was considered, probing the system to reduce dependencies on a small number of specific channels.

To demonstrate the flexibility and simplicity of SAL and LBN, we integrated it into two different classifiers. The first is a multinomial logistic regressor (LogReg) trained with 2 epochs and batch size of 1024. Secondly, we implemented the classifier from [5], which we refer to as CapgmyoNet (CpgmNet), trained with 1 epoch and a batch size of 128. As opposed to activity images, as recommended in [5], CapgmyoNet processed raw sEMG image frames. Given the findings from [14], we optimize the loss based on the sum across the batch, as opposed to the average, to leverage the linear scaling rule between learning rate and batch size and fix a learning rate for different batch sizes. For this to be valid, we also implemented a gradual warm-up learning rate schedule, where the learning rate was linearly increased from 1% to 100% of the base learning rate over the first training epoch. All classifiers were trained using the *Adam* optimizer, cross-entropy loss, and a base learning rate of 0.05.

TABLE I
INTRASESSION EXPERIMENTS (TEST ACCURACY)

	Base	Drpt.	BN	BN+Drpt.
CSL				
LogReg	0.923	0.892	0.903	0.920
CpgmNet	0.949	0.903	0.848	0.943
Capgmyo				
LogReg	0.962	0.973	0.972	0.969
CpgmNet	0.884	0.930	0.905	0.935

TABLE II
INTERSESSION EXPERIMENTS (TEST ACCURACY)

	BN	BN + Drpt.	LBN	LBN+Drpt.
CSL				
LogReg	0.147(0.126)	0.227(0.190)	-	-
LogReg(fine-tune)	0.427(0.326)	0.414(0.266)	-	-
LogReg(SAL)	0.337(0.274)	0.571(0.339)	0.555(0.404)	0.698(0.394)
CpgmNet	0.151(0.127)	0.184(0.154)	-	-
CpgmNet(fine-tune)	0.700(0.502)	0.686(0.405)	-	-
CpgmNet(SAL)	0.386(0.305)	0.604(0.425)	0.133(0.114)	0.721(0.472)
Capgmyo				
LogReg	0.439(0.436)	0.447(0.444)	-	-
LogReg(fine-tune)	0.761(0.752)	0.787(0.728)	-	-
LogReg(SAL)	0.614(0.606)	0.656(0.550)	0.723(0.714)	0.737(0.638)
CpgmNet	0.401(0.318)	0.402(0.328)	-	-
CpgmNet(fine-tune)	0.813(0.586)	0.745(0.476)	-	-
CpgmNet(SAL)	0.582(0.414)	0.535(0.375)	0.652(0.430)	0.587(0.391)

For each intrasession experimental setting, 9 repetitions of each gesture were randomly selected from a recording session for training, and evaluated on data of the left-out repetition. For each intersession experimental setting, for every permutation of 2 sessions for a subject, the model was trained on the first session, adapted on one randomly sampled repetition of each gesture from the second session, and evaluated on the remaining 9 repetitions of each gesture. For fine-tuning, all parameters were left trainable during adaptation. For SAL, as in Figure 1, all affine and LBN parameters are frozen during training, and during adaptation, all are frozen except affine and LBN parameters. Across models, the same hyperparameters in training were used during adaptation, with the number of epochs being multiplied by a factor 10, ensuring the same number of iterations as training.

III. EXPERIMENTAL ANALYSIS

A. Experiment 1: Intrasession Performance

The first experiment involves obtaining the intrasession performance scores for the aforementioned classifiers on each of the datasets, acting as a practical upper-bound for intersession performance. As shown in Table I accuracies are high across models, with the optimal condition for each model being above 93% accuracy. Interestingly, even a logistic regressor is able to achieve competitive performances, outperforming CapgmyoNet with Capgmyo data.

TABLE III
ABLATION EXPERIMENTS (TEST ACCURACY)

	LBN (no affine)	No translation	Translation only	Circumferential translation only
CSL				
LogReg	0.433(0.253)	0.497(0.281)	0.647(0.369)	0.644(0.363)
CapgmNet	0.526(0.308)	0.592(0.357)	0.723(0.468)	0.714(0.454)
Capgmyo				
LogReg	0.553(0.495)	0.628(0.544)	0.709(0.621)	0.704(0.62)
CapgmNet	0.492(0.339)	0.530(0.351)	0.577(0.367)	0.607(0.387)

B. Experiment 2: Intersession Performance

Intersession performance is measured as the accuracy from training on one session and testing on another session of the same subject. In our approach, SAL and LBN are optimized during an adaptation step, which is compared against fine-tuning. We expected that since the data from Capgmyo is not a regular grid (variable interelectrode distance), assumptions made by SAL would distort the images and not be as beneficial towards performance, whereas the regular grids used in CSL make it the ideal SAL test case. Performances reported use majority voting over the full active segment for CSL and 150ms window for Capgmyo, as in [5]. Non majority-voted performances are reported in parentheses.

From Table II, as expected, while all models achieved higher performance with fine-tuning for Capgmyo, for the regular grid data in CSL the optimal performance was achieved with SAL, despite using orders of magnitude less parameters. Furthermore, when using SAL, it can be clearly seen across models that the use of LBN significantly improves performance over traditional BN, highlighting the flexibility of learning the optimal baseline activity to subtract over estimating it directly from the data. Surprisingly, input dropout proved vital when using SAL, consistently resulting in accuracy improvements of over 20%, up to an astonishing improvement of almost 60% improvement for CapgmNet. It is likely that input dropout significantly probes the model to depend on different input combinations, reducing its likelihood of overfitting to specific channels. Additionally, while SAL leaves the original learned representation intact, further experiments showed that after fine-tuning, performance on the original training set was less than 1% higher than zero-shot intersession, indicative of catastrophic forgetting [10]. Finally, while the CNNs outperform logistic regression, it is promising to see that with SAL applying domain adaptation at the input level, even traditional, interpretable classifiers can achieve comparable performance to SOTA EMG-based classifiers.

C. Experiment 3: Model Ablation & Interpretability Assessment

Given the results from Experiment 2, we explore the importance of different affine coefficients on the final performance for each model and dataset, using input dropout and LBN. Given that the signal array geometry and often orientation

are consistent across experiments in both datasets considered, especially in sEMG, we expected that the translation parameters would be the most significant out of the 7 learnable coefficients. In addition, since electrode displacements along the circumference of the arm are most detrimental to sEMG classification performance as muscles are mostly distributed along the length of the forearm [6], [9], we expected that corrections of such translations with SAL are likely to yield the largest performance improvements.

Thus, we run an ablation experiment of SAL with four different conditions: LBN (no affine), frozen translation coefficients, all SAL coefficients frozen except for translation, and keeping only the circumferential shift parameter learnable. As in Experiment II, performances reported use majority voting over the full active segment for CSL and 150ms window for Capgmyo, as in [5]. Non majority-voted performances are reported in parentheses.

As shown in Table III, while LBN alone accounts for significant improvements, SAL accounts for the majority of the improvements with only 7 learnable parameters. Furthermore, as expected, only keeping 2 learnable translation parameters results in significantly higher performance than the remaining 5 affine parameters. In line with past studies, the performance for only circumferential translation (1 affine coefficient) is nearly identical to the performance using both translation coefficients. Thus, SAL is able to drastically improve performance using few parameters closely associated with the physical cause of performance detriments. While these trends were observed for both datasets, non-translation affine parameters seemed to account for a larger proportion of performance with Capgmyo than CSL, as they are more useful for distortions introduced by the irregular geometry of Capgmyo grids.

IV. CONCLUSION

We have shown that SAL can be prepended to any differentiable model, from a logistic regressor to CNNs, and achieve higher intersession performances than even standard fine-tuning with orders of magnitude less parameters for biosignal arrays. In addition, LBN better accounts for baseline activity fluctuations over traditional BN making it particularly well suited for biosignal sensor arrays such as sEMG. Ablation experiments suggest that learnt SAL coefficients are directly associated with the physical causes of the performance detriment. Interestingly, major improvements in sEMG systems by only accounting for circumferential translations suggest the possibility of applying the proposed approach to more practical 1D sensor arrays, such as the one in [1].

Using one repetition per class, as in this study, is commonplace in sEMG literature [5], [11], with some studies using half [12] or even all [5] of the target data for adaptation. However, this becomes impractical for large number of classes. Thus, given that SAL and LBN apply domain adaptation at an input level, and electrode displacement and baseline fluctuations being invariant to class labels, future studies will explore whether our approach can adapt to one repetition of one (or a few) class(es), unlike present domain adaptation approaches.

REFERENCES

- [1] D. Sussillo, P. Kaifosh, and T. Reardon, "A generic noninvasive neuromotor interface for human-computer interaction," 2024. [Online]. Available: <https://www.biorxiv.org/content/early/2024/07/23/2024.02.23.581779>
- [2] R. R.-M. Serrano, S. Velasco-Bosom, A. Dominguez-Alfaro, M. L. Picchio, D. Mantione, D. Mecerreyes, and G. G. Malliaras, "High density body surface potential mapping with conducting polymer-eutectogel electrode arrays for ecg imaging," *Advanced Science*, vol. 11, no. 27, p. 2301176, 2024. [Online]. Available: <https://onlinelibrary.wiley.com/doi/abs/10.1002/advs.202301176>
- [3] D. Xiong, D. Zhang, X. Zhao, and Y. Zhao, "Deep learning for emg-based human-machine interaction: A review," *IEEE/CAA Journal of Automatica Sinica*, vol. 8, no. 3, pp. 512–533, 2021.
- [4] C. Amma, T. Krings, J. Böer, and T. Schultz, "Advancing muscle-computer interfaces with high-density electromyography," in *Proceedings of the 33rd Annual ACM Conference on Human Factors in Computing Systems*, ser. CHI '15. New York, NY, USA: ACM, 2015, pp. 929–938. [Online]. Available: [10.1145/2702123.2702501](https://doi.acm.org/10.1145/2702123.2702501)
- [5] Y. Du, W. Jin, W. Wei, Y. Hu, and W. Geng, "Surface emg-based inter-session gesture recognition enhanced by deep domain adaptation," *Sensors*, vol. 17, no. 3, 2017. [Online]. Available: <https://www.mdpi.com/1424-8220/17/3/458>
- [6] L. Hargrove, K. Englehart, and B. Hudgins, "A training strategy to reduce classification degradation due to electrode displacements in pattern recognition based myoelectric control," *Biomedical Signal Processing and Control*, vol. 3, no. 2, pp. 175–180, 2008, surface Electromyography. [Online]. Available: <https://www.sciencedirect.com/science/article/pii/S1746809407001012>
- [7] H. Kim and C.-H. Im, "Influence of the number of channels and classification algorithm on the performance robustness to electrode shift in steady-state visual evoked potential-based brain-computer interfaces," *Front. Neuroinform.*, vol. 15, p. 750839, Oct. 2021.
- [8] F. Wang, M. Mao, L. Duan, Y. Huang, Z. Li, and C. Zhu, "Intersession instability in fnirs-based emotion recognition," *IEEE Transactions on Neural Systems and Rehabilitation Engineering*, vol. 26, no. 7, pp. 1324–1333, 2018.
- [9] J. Pereira, D. Halatsis, B. Hodossy, and D. Farina, "Tackling electrode shift in gesture recognition with hd-emg electrode subsets," in *ICASSP 2024 - 2024 IEEE International Conference on Acoustics, Speech and Signal Processing (ICASSP)*, 2024, pp. 1786–1790.
- [10] U. Cote-Allard, C. L. Fall, A. Drouin, A. Campeau-Lecours, C. Gosselin, K. Glette, F. Laviolette, and B. Gosselin, "Deep learning for electromyographic hand gesture signal classification using transfer learning," *IEEE Transactions on Neural Systems and Rehabilitation Engineering*, vol. 27, no. 4, p. 760–771, 2019.
- [11] X. Fan, L. Zou, Z. Liu, Y. He, L. Zou, and R. Chi, "Csac-net: Fast adaptive semg recognition through attention convolution network and model-agnostic meta-learning," *Sensors*, vol. 22, no. 10, 2022. [Online]. Available: <https://www.mdpi.com/1424-8220/22/10/3661>
- [12] I. Ketykó, F. Kovács, and K. Z. Varga, "Domain adaptation for semg-based gesture recognition with recurrent neural networks," in *2019 International Joint Conference on Neural Networks (IJCNN)*, 2019, pp. 1–7.
- [13] M. Jaderberg, K. Simonyan, A. Zisserman, and K. Kavukcuoglu, "Spatial transformer networks," 2016. [Online]. Available: <https://arxiv.org/abs/1506.02025>
- [14] P. Goyal, P. Dollár, R. B. Girshick, P. Noordhuis, L. Wesolowski, A. Kyrola, A. Tulloch, Y. Jia, and K. He, "Accurate, large minibatch SGD: training imagenet in 1 hour," *CoRR*, vol. abs/1706.02677, 2017. [Online]. Available: <http://arxiv.org/abs/1706.02677>